Am J Physiol Endocrinol Metab 308: E294–E305, 2015.
First published December 9, 2014; doi:10.1152/ajpendo.00189.2014.

The cholesterol-lowering agent methyl-β-cyclodextrin promotes glucose uptake via GLUT4 in adult muscle fibers and reduces insulin resistance in obese mice

Paola Llanos,[1,2] Ariel Contreras-Ferrat,[1,2] Tihomir Georgiev,[3] Cesar Osorio-Fuentealba,[4] Alejandra Espinosa,[1] Jorge Hidalgo,[1,5] Cecilia Hidalgo,[1,5,6] and Enrique Jaimovich[1,7]

[1]*Center for Molecular Studies of the Cell, Facultad de Medicina, Universidad de Chile, Santiago, Chile;* [2]*Institute for Research in Dental Sciences, Facultad de Odontología, Universidad de Chile, Santiago, Chile;* [3]*Medical Biophysics, Institute of Physiology und Pathophysiology, Ruprecht Karls Universität, Heidelberg, Germany;* [4]*Laboratorio de Bionanotecnología, Universidad Bernardo O'Higgins, Santiago, Chile;* [5]*Physiology and Biophysics Program, Institute of Biomedical Sciences (ICBM), Facultad de Medicina, Universidad de Chile, Santiago, Chile;* [6]*Biomedical Neuroscience Institute, Facultad de Medicina, Universidad de Chile, Santiago, Chile; and* [7]*Cell and Molecular Biology Program, ICBM, Facultad de Medicina, Universidad de Chile, Santiago, Chile*

Submitted 17 April 2014; accepted in final form 6 December 2014

Llanos P, Contreras-Ferrat A, Georgiev T, Osorio-Fuentealba C, Espinosa A, Hidalgo J, Hidalgo C, Jaimovich E. The cholesterol-lowering agent methyl-β-cyclodextrin promotes glucose uptake via GLUT4 in adult muscle fibers and reduces insulin resistance in obese mice. *Am J Physiol Endocrinol Metab* 308: E294–E305, 2015. First published December 9, 2014; doi:10.1152/ajpendo.00189.2014.—Insulin stimulates glucose uptake in adult skeletal muscle by promoting the translocation of GLUT4 glucose transporters to the transverse tubule (T-tubule) membranes, which have particularly high cholesterol levels. We investigated whether T-tubule cholesterol content affects insulin-induced glucose transport. Feeding mice a high-fat diet (HFD) for 8 wk increased by 30% the T-tubule cholesterol content of triad-enriched vesicular fractions from muscle tissue compared with triads from control mice. Additionally, isolated muscle fibers (flexor digitorum brevis) from HFD-fed mice showed a 40% decrease in insulin-stimulated glucose uptake rates compared with fibers from control mice. In HFD-fed mice, four subcutaneous injections of MβCD, an agent reported to extract membrane cholesterol, improved their defective glucose tolerance test and normalized their high fasting glucose levels. The preincubation of isolated muscle fibers with relatively low concentrations of MβCD increased both basal and insulin-induced glucose uptake in fibers from controls or HFD-fed mice and decreased Akt phosphorylation without altering AMPK-mediated signaling. In fibers from HFD-fed mice, MβCD improved insulin sensitivity even after Akt or CaMK II inhibition and increased membrane GLUT4 content. Indinavir, a GLUT4 antagonist, prevented the stimulatory effects of MβCD on glucose uptake. Addition of MβCD elicited ryanodine receptor-mediated calcium signals in isolated fibers, which were essential for glucose uptake. Our findings suggest that T-tubule cholesterol content exerts a critical regulatory role on insulin-stimulated GLUT4 translocation and glucose transport and that partial cholesterol removal from muscle fibers may represent a useful strategy to counteract insulin resistance.

glucose transporter 4; ryanodine receptor; calcium; transverse tubules; high-fat diet; diabetes

THE SKELETAL MUSCLE TISSUE plays a critical role in body energy balance and glucose homeostasis. Under postprandial conditions, skeletal muscle accounts for about 80% of plasma glucose removal; this tissue is also a major consumer of fatty acids, which together with glucose constitute the principal energy sources of muscle tissue (58). The ability of skeletal muscle to switch between glucose and fatty acids as primary energy sources is central to the regulation of whole body energy balance. Skeletal muscle and fat tissue are the principal insulin-sensitive targets in the body and represent the main sites of insulin-mediated glucose metabolism. Insulin exerts its effects via a complex cascade of signaling events. Alterations in these signaling pathways lead to insulin resistance, defined as a defect in insulin-stimulated glucose disposal by peripheral tissues, which is a rapidly growing health problem worldwide (11). Increased plasma levels of free fatty acids, fat-rich diets, and glucose infusion all cause insulin resistance (54). The detailed mechanisms underlying insulin resistance are unknown, but several defects in insulin signaling have been reported for this condition (45, 51).

Considering the significant contribution of skeletal muscle to total body energy usage, an impaired metabolic response of skeletal muscle is closely associated with the onset of the metabolic syndrome to insulin resistance and type 2 diabetes mellitus. The reduction of glucose uptake and impaired glucose metabolism are characteristic features of insulin-resistant skeletal muscle, where most plasma glucose is normally destined during insulin stimulation. Muscle insulin resistance arises in conditions of high fatty acid availability and correlates with triglyceride accumulation within skeletal muscle fibers (29). A key mechanism leading to intramuscular triglyceride accumulation may be the failure of obese subjects with insulin resistance and type 2 diabetes to activate fatty acid oxidation by switching energy substrate utilization (28).

Thirteen members of the glucose transporter (GLUT) family mediate glucose transport through the plasma membrane (25). In particular, the GLUT4 transporter is expressed solely in skeletal and cardiac striated muscles and in adipose tissue (25). Skeletal muscle cells have a complex membrane system comprised of the surface membrane plus the membrane invaginations that originate the transverse tubule (T-tubule) system, which has a total membrane area that is severalfold larger than the surface membrane. In the basal state, GLUT4 is stored predominantly in intracellular vesicles. Upon stimulation,

Address for reprint requests and other correspondence: P. Llanos, Inst. for Research in Dental Sciences, Facultad de Odontología, Universidad de Chile, Sergio Livingstone Pohlhammer 943, Independencia, Santiago, Chile (e-mail: pllanos@med.uchile.cl).

these vesicles translocate to the muscle plasma membrane system, where GLUT4 insertion increases glucose uptake (6, 25, 33, 59). In skeletal muscle, both insulin and exercise stimulate GLUT4 recruitment to the plasma membrane, although they engage in partially different signaling pathways (6, 44, 59).

Several studies involve changes in free cytoplasmic Ca^{2+} concentration ($[Ca^{2+}]_i$) in the insulin-signaling pathway. In striated muscle, $[Ca^{2+}]_i$ is tightly controlled in terms of spatial and temporal distribution, and both chemical and electrical signaling modulate the intracellular Ca^{2+} levels (2). Studies to elucidate the effects of insulin on $[Ca^{2+}]_i$ performed on isolated, intact flexor digitorum brevis (FDB) fibers from mouse and rat (4, 5) indicate that there is a marked increase in $[Ca^{2+}]_i$ close to the plasma membrane due to Ca^{2+} entry into the cell, which depends on phosphoinositide 3-kinase (PI3K) activity (4). We have reported previously that insulin addition to skeletal myotubes produces a fast intracellular Ca^{2+} transient that requires extracellular Ca^{2+}; both the L-type Ca^{2+} channel blocker nifedipine and μM ryanodine, which prevents Ca^{2+} release mediated by the ryanodine receptor (RyR), inhibit this Ca^{2+} transient (14). Other reports show that the $[Ca^{2+}]_i$ increase evoked by insulin in skeletal muscle fibers depends on Ca^{2+} influx and is related to GLUT4 translocation (32). Yet the detailed mechanisms whereby the insulin-dependent Ca^{2+} transient contributes to enhance glucose transport remain unknown.

The physiological relevance of plasma membrane cholesterol levels has attracted increased attention in recent years. Biochemical and structural studies have indicated that the T-tubule and the surface plasma membrane of mammalian skeletal muscle differ in lipid composition, with fourfold higher cholesterol content in the T-tubules relative to the plasma membrane (34, 49, 56). At physiological temperature, the lipid phase of T-tubules is significantly less fluid than in most mammalian plasma membranes (21), a feature that may arise from its high cholesterol content. Previous reports indicate that feeding both mice and Ossabaw swine a high-fat diet (HFD) increases cholesterol levels in skeletal muscle plasma membranes (19). Moreover, recent studies report that the increased GLUT4 translocation produced by moderate cholesterol loss in both L6 myotubes (19) and cultured adipocytes (37) does not involve known insulin-signaling proteins.

In this work, we evaluated in mice the effects of modifying cholesterol levels on glucose handling and on GLUT4 translocation, glucose uptake, and Ca^{2+} signal generation in single fibers isolated from adult skeletal muscle. Subcutaneous injections of methyl-β-cyclodextrin (MβCD) to HFD-fed mice improved the glucose tolerance test and restored fasting glucose to normal levels; significantly, exposure of fibers from mice fed a HFD to MβCD resulted in enhanced insulin-induced GLUT4 translocation and increased glucose uptake.

MATERIALS AND METHODS

Animals Male C57BL/6J mice were obtained from the Animal Facility at the Faculty of Medicine, Universidad de Chile. Room temperature was kept constant at 21°C, and light was maintained on a 12:12-h light-dark cycle. At 20 days old, mice were divided into two groups. The control (NCD) group received a diet containing (wt/wt) 10% fat, 20% protein, and 70% carbohydrate. The group fed a HFD received a diet containing (wt/wt) 60% fat, 20% protein, and 20% carbohydrate (D12492; Research Diets, New Brunswick, NJ). Animals were euthanized after 8 wk of treatment. A subgroup of HFD-fed mice was injected subcutaneously with 500 mg/kg MβCD or saline twice/wk for 2 wk. The Bioethics Committee of the Faculty of Medicine, Universidad de Chile, approved all animal procedures performed in this work.

Biochemical determinations. An intraperitoneal glucose tolerance test was performed after 12–16 h of fasting by administration of a glucose bolus of 2 g/kg. At 0, 15, 30, 60, and 120 min, tail blood samples were obtained. Blood glucose concentrations were measured on a Johnson & Johnson's OneTouch Glucometer. Plasma insulin concentrations were determined with a commercially available immunoassay specific for mice (Mercodia, Uppsala, Sweden). Other biochemical parameters were measured according to the manufacturer's instructions.

Cultures of adult skeletal muscle fibers. Eight-week-old mice were used throughout this work. The isolation procedure was described previously (8). Briefly, isolated fibers from FDB muscle were obtained by enzymatic digestion for 90 min at 37°C of the whole muscle with collagenase type 2 (Worthington, Lakewood, NJ). Afterward, the muscle was mechanically dissociated by passage through fire-polished Pasteur pipettes. Isolated fibers were seeded in matrigel-coated coverslips in Dulbecco's modified Eagle's medium (Invitrogen, Carlsbad, CA) supplemented with 10% horse serum (Invitrogen). Fibers were used for experimentation no more than 8 h after isolation.

Triad isolation and measurement of cholesterol content. Isolation of triad-enriched fractions from gastrocnemius or tibialis anterior muscles derived from 8-wk-old NCD or HFD-fed mice was performed using differential centrifugation, as standardized previously in our laboratory for frog and rabbit muscles (22). Cholesterol content was measured with a colorimetric Cholesterol Assay Kit (Winner) or Amplex Red Cholesterol Assay Kit (Invitrogen) and was normalized by protein concentration.

Single-fiber assay of fluorescent 2-NBDG uptake. The procedure followed to determine the uptake of fluorescent 2-[N-(7-nitrobenz-2-oxa-1,3-diazol-4-yl)amino]-2-deoxy-D-glucose (2-NBDG) was described previously (44). Briefly, muscle fibers were washed with Krebs-Ringer buffer and stimulated with 100 nM insulin for 20 min. Single fibers were exposed for 15 min to 300 μM 2-NBDG and were rinsed with Krebs buffer before stimulation. Individual fibers were excited with a 488-nm Argon laser line, and the fluorescence emission collected with a ×40 Plan Apofluo objective was band pass filtered between 505 and 550 nm in a confocal Carl Zeiss Pascal 5 microscope. Hexose uptake was estimated by comparison of the intracellular fluorescent signal with the extracellular signal. For each condition, 20 single fibers per culture were analyzed. Regions of interest of the images were quantified by ImageJ software (National Institutes of Healths, Bethesda, MD).

Western blot analysis. FDB muscles from mice were homogenized by sonication in cold lysis buffer (140 mM NaCl; 1% Triton X-100, 1 mM EDTA, 1 mM EGTA, and 20 mM Tris·HCl, pH 7.5) supplemented with protease and phosphatase inhibitors. Samples were incubated on ice for 30 min, and after centrifugation for 30 min at 3,000 *g*, supernatant proteins were separated on 12% SDS-PAGE gels. After transference to a polyvinylidene difluoride membrane, incubations with primary antibodies were maintained at 4°C overnight. The primary antibodies used were anti-Akt (1:1,000), anti-phospho-Akt (Ser^{473}, 1:1,000), and anti-phospho-AMPK (Thr^{172}, 1:1,000); all three antibodies were from Cell Signaling Technology (Danvers, MA), and anti-β-tubulin (1:1,000) was from Sigma-Aldrich (St. Louis, MO). After washing, membranes were incubated for 1.5 h with secondary, anti-rabbit or anti-mouse antibodies (Sigma-Aldrich).

Cell surface GLUT4 detection assays. The presence of GLUT4 at the fiber surface was assessed by measuring both biotinylation for the endogenous transporter and translocation of the GLUT4*myc*-eGFP chimera to the sarcolemma. Briefly, fibers were washed three times in

PBS at 4°C, and then sulfo-NHS-Biotin (Thermo Scientific, Rockford, IL) was added to a final concentration of 0.5 mg/ml for 1 h; 100 mM glycine was added to neutralize biotin. Fibers were lysed as described above, and protein content was quantified with BCA protein assay kit (Thermo Scientific). Samples containing the same protein concentration were incubated overnight at 4°C (under constant stirring) with NeutrAvidin plus ultralink resin (Thermo Scientific) and then centrifuged at 14,000 rpm for 15 min. The nonbiotinylated fraction remained in the supernatant and the biotinylated fraction in the pellet. Both fractions were collected, resuspended in Laemmli buffer, and incubated at 65°C for 30 min. In the biotinylated fraction, the beads were once again briefly centrifuged, and the supernatants containing solubilized plasma membrane proteins were removed and frozen until they were ready to use. The proteins present in both fractions were separated by electrophoresis in 12% polyacrylamide gels, and GLUT4 content was determined by Western blot analysis with a polyclonal GLUT4 antibody (Santa Cruz Biotechnology, Dallas, TX). Intramuscular plasmid injection and electroporation were performed as described previously (13). Briefly, mice were anesthetized with isofluorane and injected with hyaluronidase (2 mg/ml) in 0.9% NaCl. After recovery for 1 h, the plasmidial construct was injected and electroporation performed using 100 mV, 1 Hz, 20 ms, and 20 times protocol. Then, the mice were allowed to rest for 2 wk before the experiments.

Immunofluorescence. Fibers plated on 35-mm coverslips were preincubated for 20 min with 0.76 mM MβCD, 100 nM insulin, or both. After washing with PBS, fibers were fixed by incubation for 10 min at room temperature with PBS containing 4% paraformaldehyde (Electron Microscopy Science, Hatfield, PA). Next, fibers were rinsed with PBS, permeabilized with 0.1% Triton X-100 in PBS, rinsed with PBS, and blocked for 1 h with PBS-1% BSA at room temperature. Monoclonal antibodies against mouse GLUT4 (1:500; Cell Signaling Technology) were used to detect GLUT4 distribution. Fibers were washed and then incubated for 1 h with Alexa Fluor 488 anti-mouse antibody (Molecular Probes Invitrogen). Samples were treated with Dako anti-fading reagent (Dako) and stored at 4°C until use.

Calcium signal detection. Isolated FDB fibers were incubated for 30 min with 5 μM fluo 4-AM at room temperature in standard Krebs buffer; at this point, 0.76 mM MβCD was added to the recording chamber for fluorescence image capture every 5 s. The image series during experiments were obtained with a confocal microscope (Carl Zeiss Axiovert 200M, LSM Pascal5). The fluorophore was excited with an Argon laser at 488 nm, and fluorescence images were collected every 1.0–2.0 s (corresponding to exposure time for each image) and analyzed frame by frame. The average fiber fluorescence (F) was calculated for each image on an outline of the fiber and was normalized to its initial or preintervention F_0 value, as F/F_0.

Statistical analysis. Data are presented as means ± SE. Significant differences between and within multiple groups were examined using ANOVA for repeated measurements, followed by Tukey multiple comparison test. Student's *t*-test was used to detect significant differences between two groups. $P < 0.05$ was considered statistically significant.

RESULTS

Altered body weight, body fat content, and metabolic status in HFD-fed mice. We monitored for an 8-wk period the body weight, body fat content, and metabolic variables in both HFD-fed and NCD-fed mice. Mice fed a HFD showed progressive weight gain compared with NCD-fed animals, reaching an average body weight (in g) of 32.5 ± 1.9 and 22.9 ± 0.6, respectively, at 8 wk (Fig. 1, *A* and *B*). In addition, HFD-fed mice showed significantly altered glucose tolerance test compared with control mice (Fig. 1*C*) and elevated fasting serum glucose levels relative to controls with values (mg/dl) of 215.3 ± 17.5 and 133.8 ± 6.1, respectively (Fig. 1*D*). In HFD-fed mice, fasting insulin levels were also higher than in control animals, with values (mU/ml) of 11.9 ± 2.7 and 4.8 ± 1.3, respectively (Fig. 1*E*). The average HOMA-IR value for HFD-fed mice was 6.4 ± 1.3; this value was threefold higher than the value of 1.9 ± 0.5 determined in control mice (Fig. 1*F*). We also evaluated body fat distribution, finding an increase in white and brown fat in HFD-fed mice compared with control animals (Fig. 1*G*). The plasma triglyceride concentration of HFD-fed mice reached an average value of 0.74 ± 0.1 g/l, which was twofold higher than the average value of 0.35 ± 0.04 g/l determined in control mice (Fig. 1*H*). Plasma cholesterol levels were also elevated in HFD-fed mice compared with their controls, yielding values (g/l) of 0.95 ± 0.13 and 0.66 ± 0.05, respectively (Fig. 1*I*). In basal conditions, the incorporation of 2-NBDG in muscle fibers from HFD-fed mice (HFD-fibers from now on) was lower (0.87 ± 0.07-fold) than in fibers from NCD-fed mice. Pretreatment of fibers from NCD-fed mice with 100 nM insulin significantly increased 2-NBDG uptake by 1.80 ± 0.04-fold relative to their basal condition (Fig. 1*J*, open bars). For comparison, insulin produced minor (1.17 ± 0.05-fold) stimulation of glucose uptake in fibers from HFD-fed mice (Fig. 1*J*, black bars). Taken together, these results suggest that HFD-fed mice exhibit severe insulin resistance and thus represent a good model for this study.

MβCD treatment improves the glucose tolerance test and restores fasting glucose levels and insulin-stimulated 2-NBDG uptake in HFD-fed mice. To investigate the effects of MβCD, a dextrin that partially removes cholesterol from membranes, on glucose homeostasis in vivo, we performed experiments in HFD-fed mice injected subcutaneously with this drug. For 2 wk, HFD-fed mice (8 wk old) were injected subcutaneously twice/wk with MβCD (500 mg/kg) or saline. Mice injected with either MβCD or saline displayed similar food intake, body weight, and movement capacity throughout the experimental period and were found to be similar in both groups (data no shown). In the random displacement test, there was a tendency of the injected animals to exhibit a reduced total trajectory, but this point was not further studied. The intraperitoneal glucose tolerance test was performed on fasted (16 h) mice injected with 2 g/kg intraperitoneal glucose. Figure 2 shows that treatment with MβCD restored fasting blood glucose to control levels, which remained significantly high in sham-injected mice, and significantly improved the glucose tolerance test. Fasting plasma glucose levels (mg/dl) were 127 ± 10.9 in NCD-fed mice, 121 ± 5 in HFD-fed mice injected (4 times) with MβCD, and 166 ± 8.9 in sham-injected HFD-fed mice (Fig. 2*B*). After the fourth subcutaneous MβCD injection, HFD-fed mice displayed an improved response in the glucose tolerance test compared with sham-injected mice, with plasma glucose levels at 60 min of 262.5 ± 9.8 and 389 ± 44.7, respectively (Fig. 2*A*). Taken together, these results strongly suggest that MβCD exerts hypoglycemic effects in insulin-resistant mice. In addition, insulin significantly stimulated 2-NBDG uptake in fibers isolated from MβCD-injected HFD-fed mice (Fig. 2*C*), which increased from 0.91 ± 0.03-fold in basal conditions to 1.31 ± 0.04-fold in the presence of insulin (Fig. 2*C*, black bars). In contrast, sham-injected mice yielded values of 0.99 ± 0.03-fold stimulation in basal conditions and 1.05 ± 0.03 in the presence of insulin (Fig. 2*C*, open bars).

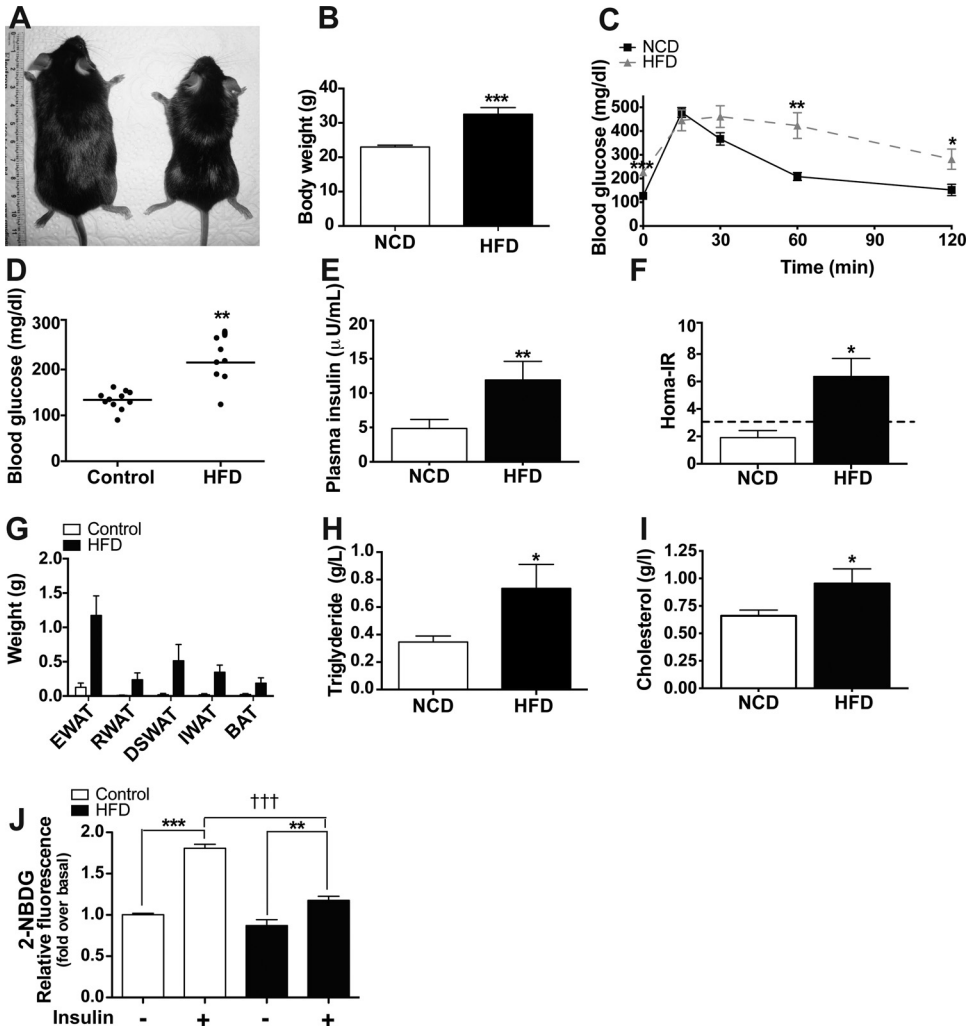

Fig. 1. High-fat diet (HFD)-fed mice showed alterations in body weight, body fat content, and metabolic variables. *A*: illustrative images of 8-wk-old normal mice fed either a control diet (NCD; *right*) or a 60% fat diet (HFD; *left*). *B*: HFD-fed mice ($n = 8$) showed significantly increased body weight compared with control mice ($n = 10$). *C*: glucose tolerance test (GTT). HFD-fed mice ($n = 5$) displayed altered GTT relative to control mice ($n = 6$). *D*: fasting blood glucose levels in HFD-fed mice ($n = 8$) and NCD mice ($n = 11$). *E*: fasting plasma insulin levels in HFD-fed mice ($n = 4$) and NCD mice ($n = 4$). *F*: homeostasis model assessment of insulin resistance (HOMA-IR) in HFD-fed ($n = 4$) and NCD mice ($n = 5$). *G*: weight of epididymal (EWAT), retroperitoneal (RWAT), dorsosubcutaneous (DSWAT), and inguinal white adipose tissue (IWAT) and of brown adipose tissue (BAT) isolated from NCD ($n = 5$) or HFD-fed mice ($n = 6$). HFD-fed mice displayed increased WAT and BAT mass compared with NCD mice. *H*: plasma triglyceride levels in NCD ($n = 8$) and HFD-fed mice ($n = 5$). *I*: plasma cholesterol levels determined in NCD ($n = 7$) and HFD-fed mice ($n = 5$). All data represent means ± SE. In *A–I*, $*P < 0.05$, $**P < 0.01$, and $***P < 0.001$, evaluated by Student's *t*-test. *J*: 2-[N-(7-nitrobenz-2-oxa-1,3-diazol-4-yl)amino]-2-deoxy-D-glucose (2-NBDG) uptake in isolated fibers from NCD and HFD-fed mice. Open bars, NCD fiber; black bars, HFD fiber ($n = 5$; means ± SE) $***P < 0.0001$, $**P < 0.001$, and $†††P < 0.0001$, evaluated by 1-way ANOVA, followed by Tukey's post-test.

Acute treatment with MβCD reduced plasma glucose levels 1 and 24 h after a single injection (Fig. 2*D*).

Cholesterol accumulation in triads from HFD-fed mice. We isolated triad-enriched vesicular fractions (from now on, designated solely as triads) from gastrocnemius or tibialis anterior muscle from NCD- or HFD-fed mice. These triad fractions contain 10% T-tubule vesicles (22), which supply a large fraction of the total cholesterol content of these fractions. In both muscle types, triads isolated from HFD-fed mice displayed a significant increase of ~30% in cholesterol content compared with triads from NCD-fed mice (Table 1). This result suggests that muscle fibers from HFD-fed mice accumulate cholesterol in their T-tubule membranes.

MβCD increases 2-NBDG uptake in isolated adult muscle fibers. To evaluate the acute effects of MβCD on glucose homeostasis in vitro, we measured the uptake of 2-NBDG in isolated adult muscle fibers. As shown in Fig. 3*A*, MβCD concentrations (≥100 μM) increased 2-NBDG uptake in fibers from NCD-fed mice. Treatment with 0.76 mM MβCD increased glucose uptake without modifying membrane potential, which remained constant for ≤20 min after the addition of 0.76 mM MβCD (Fig. 3*B*). A higher concentration of MβCD (7.6 mM) caused membrane depolarization (data not shown). Representative confocal images of adult fibers from both NCD- and HFD-fed mice illustrate the stimulatory effects of MβCD on 2-NBDG uptake (Fig. 3*C*). Pretreatment of fibers from NCD-fed mice with 0.76 mM MβCD increased 2-NBDG uptake significantly by 1.64 ± 0.09-fold in basal conditions and by 2.21 ± 0.15-fold in the presence of insulin. Preincubation of fibers from HFD-fed mice with MβCD increased 1.90 ± 0.17-fold the incorporation of 2-NBDG in the basal condition and 2.58 ± 0.14-fold in the presence of insulin (Fig. 3, *C* and *D*). Overall, these results strongly suggest that MβCD enhances glucose uptake in fibers from both NCD- and HFD-fed mice. It is worth mentioning that although insulin enhanced the incorporation of 2-NBDG in fibers treated with MβCD, the effects of MβCD and insulin were not strictly additive.

To assess the specificity of the effect of MβCD on glucose uptake, we evaluated the effect of α-cyclodextrin (αCD), a cyclodextrin that does not bind cholesterol (43). Figure 3*E* shows that αCD did not modify glucose uptake in muscle fibers in basal conditions. Yet preincubation of fibers from NCD-fed mice with αCD produced a significant decrease in insulin-stimulated glucose uptake, which reached values 1.30 ± 0.06-fold higher than controls, significantly lower than the 1.80 ± 0.20-fold stimulation produced by insulin in fibers from NCD-fed mice not treated with αCD (Fig. 3*E*). In contrast, αCD did not modify glucose uptake in muscle fibers from HFD-fed

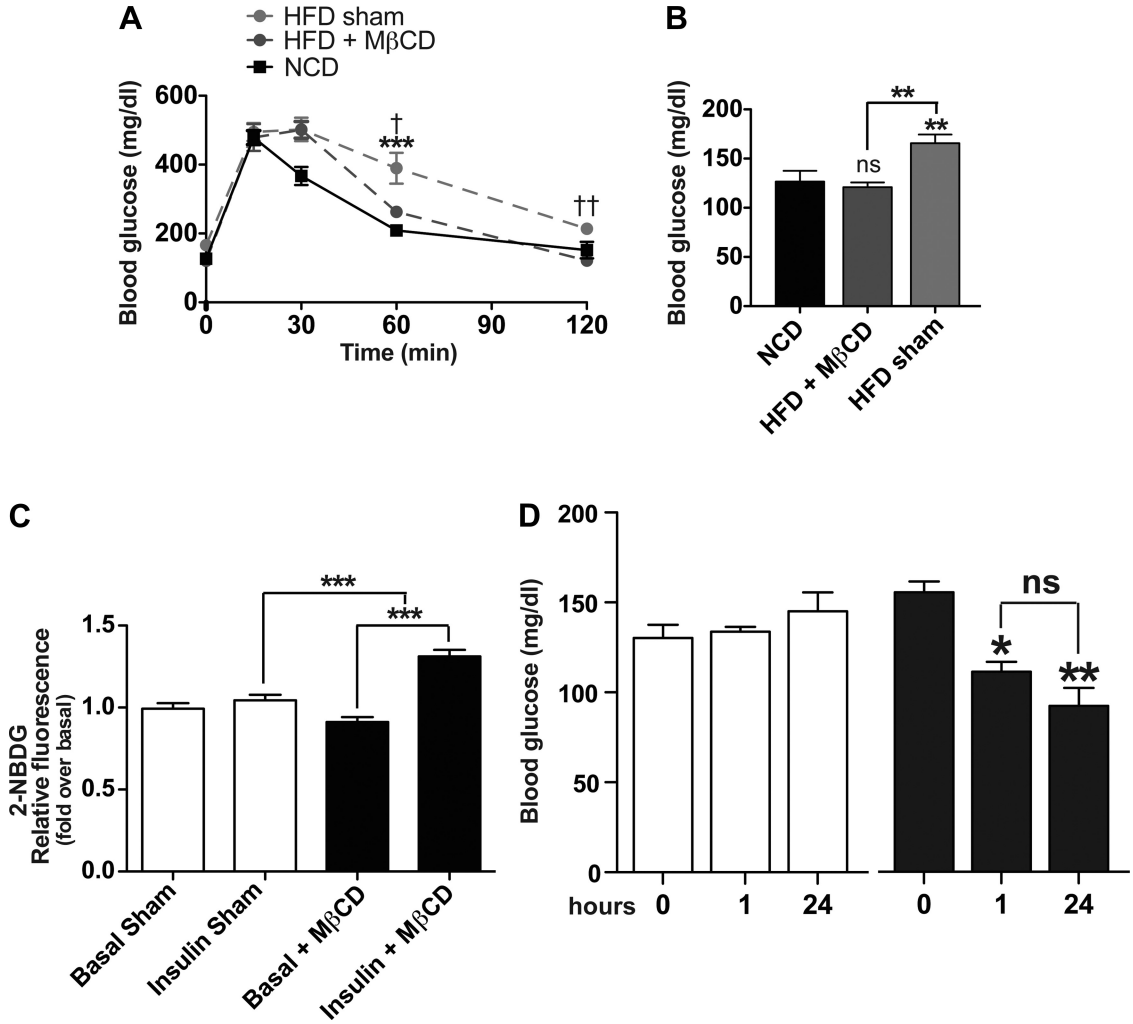

Fig. 2. Injection of methyl-β-cyclodextrin (MβCD) to HFD-fed mice improves intraperitoneal glucose tolerance test (IPGTT) and restores fasting blood glucose and insulin-stimulated glucose uptake in muscle fibers. *A*: mice were injected subcutaneously twice/wk for 2 wk with 500 mg/kg MβCD or saline, and IPGTT was performed on fasted (16 h) mice injected ip with 2 g/kg glucose. The graph shows the IPGTT curves of NCD or HFD mice or HFD mice after receiving MβCD injections ($n = 6$). *B*: fasting blood glucose levels in HFD-fed sham and HFD-fed mice injected with MβCD as in *A* ($n = 6$). Values represent means ± SE. $^{**}P < 0.01$, determined by Student's *t*-test. NS, not significant. *C*: 2-NBDG uptake in muscle fibers from HFD-fed (sham, open bars; $n = 3$) and HFD-fed mice injected with MβCD (black bars; $n = 4$). *D*: acute effects of MβCD injection on blood glucose levels. Samples were taken at 0, 1, and 24 h in HFD-fed mice injected with saline solution (sham; open bars) or with MβCD (black bars). Values represent means ± SE ($n = 3$). $^{***}P < 0.0001$, determined by 1-way ANOVA plus Tukey's posttest.

mice, either under basal conditions or following insulin addition, with relative fluorescence values of 0.80 ± 0.04 in basal conditions, 0.80 ± 0.03 in fibers preincubated with αCD, 1.10 ± 0.03 in insulin-stimulated fibers, and 0.90 ± 0.04 in fibers preincubated with αCD and stimulated with insulin. A previous report showed that αCD is effective in the removal of membrane phospholipids (26); this feature may contribute to the explanation of the decreased uptake of glucose in insulin-stimulated muscle fibers from NCD-fed mice treated with αCD. In addition, to rule out any nonspecific effect of MβCD, we assayed the effects of MβCD already loaded with cholesterol (Chol/MβCD, water-soluble cholesterol). Preincubation with 0.4 mg/ml Chol/MβCD for 30 min decreased 2-NBDG uptake significantly in basal and insulin-stimulated conditions (Fig. 3*F*), suggesting a specific effect of MβCD on glucose transport.

Table 1. *Cholesterol content in skeletal muscle triads from control and HFD-fed mice*

Muscle	NCD, μg cholesterol/mg protein	HFD, μg cholesterol/mg protein
Tibialis anterior	6.70 ± 0.12	9.20 ± 0.89*
Gastrocnemius	5.52 ± 0.17	7.50 ± 0.82*

Values are means ± SE; $n = 4$. HFD, high-fat diet; NCD, controls. Cholesterol concentration was determined enzymatically in triad fractions prepared from gastrocnemius or tibialis anterior muscles. HFD-fed animals displayed increased cholesterol content compared with controls. $^{*}P < 0.01$, Student's *t*-test.

We evaluated cholesterol levels after treatment of adult fibers with MβCD. We found that incubation with MβCD decreased by 35.4 and 42.5% the cholesterol content in fibers from NCD- and HFD-fed mice, respectively (Table 2). Taken together, these results suggest that cholesterol removal from muscle fibers increases both basal and insulin-stimulated glu-

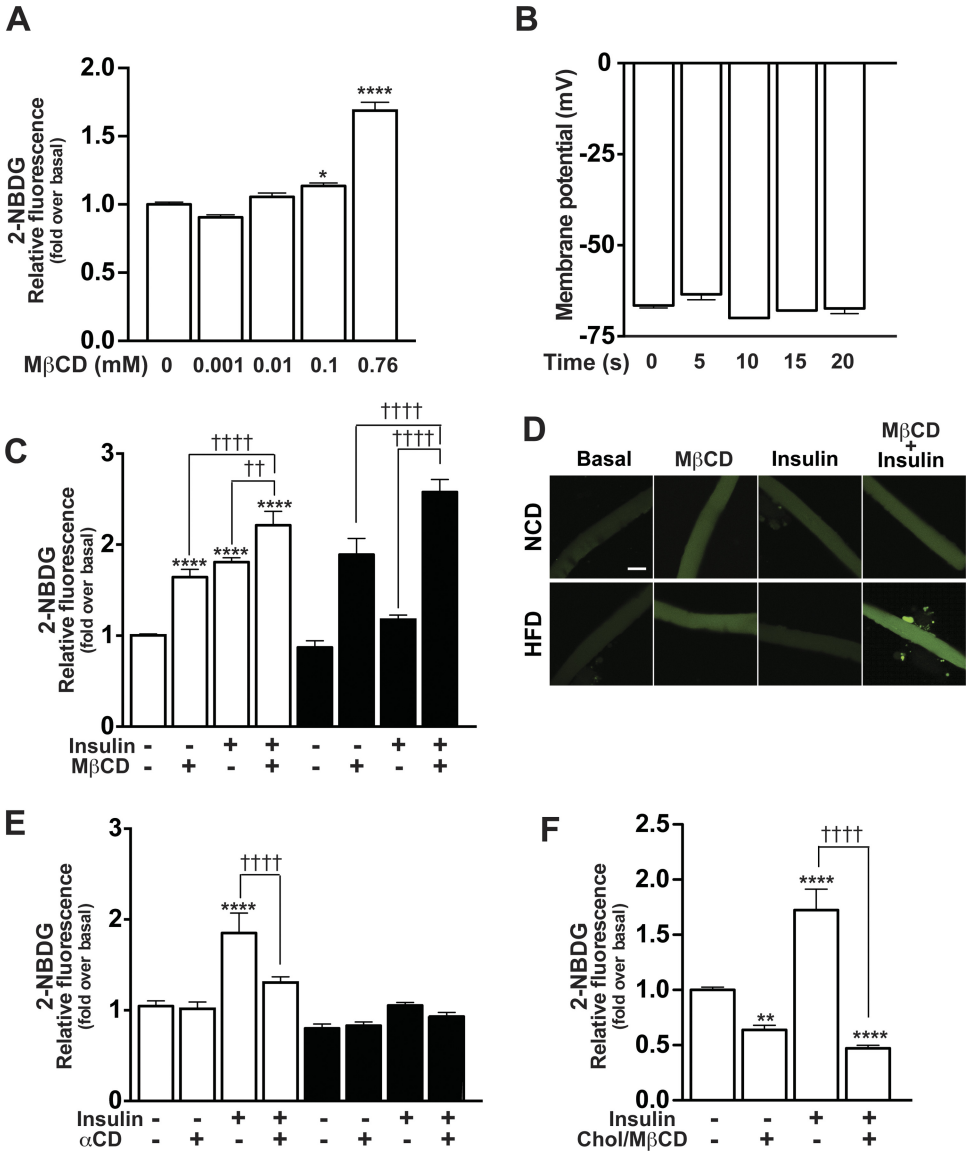

Fig. 3. MβCD increases 2-NBDG uptake in NCD and HFD-fed mice. Single fibers loaded for 15 min with 300 μM 2-NBDG were preincubated for 20 min with 100 nM insulin + MβCD or α-cyclodextrin (αCD), as indicated. *A*: dose-dependent effects of MβCD ($n = 3$). *B*: resting membrane potential ($n = 3$) in NCD fibers treated with 0.76 mM MβCD. *C*: effects of 0.76 mM MβCD on probe fluorescence; similar results were observed in 3–5 independent fiber cultures. *D*: representative confocal images of 2-NBDG uptake from isolated fibers. *E*: effects of 0.76 mM αCD on 2-NBDG fluorescence ($n = 3$). *F*: effects of 400 mg/ml cholesterol (Chol)/MβCD on 2-NBDG fluorescence ($n = 3$). Open bars, NCD fibers; black bars, HFD fibers. Values are means ± SE. ****$P < 0.0001$ vs. basal condition; ††††$P < 0.0001$, determined by 1-way ANOVA, followed by Tukey's posttest.

cose uptake in mice fed either control or HFD diets, improving insulin sensitivity, especially in the latter animals, which are significantly insulin resistant.

The increased 2-NBDG uptake induced by MβCD persists after Akt or CaMK II/AMPK inhibition. To assess whether the MβCD-dependent increase in glucose incorporation involves Akt signaling pathways (the canonical pathways of insulin signaling) and/or AMPK-mediated signaling (involving metabolism and hypoxia-activated pathways), we preincubated fibers with pharmacological inhibitors of each protein kinase. To inhibit Akt activity, we used Akt inhibitor VIII, a membrane-permeable compound that allosterically and selectively inhibits this kinase in reversible fashion (17). Fibers from NCD-fed mice yielded values of 2.50 ± 0.16- and 2.40 ± 0.24-fold stimulation after preincubation with MβCD plus Akt inhibitor VIII or with MβCD plus insulin and Akt inhibitor VIII, respectively (Fig. 4*A*, open bars), whereas in HFD fibers the corresponding values were 2.60 ± 0.14 and 2.20 ± 0.16 (Fig. 4*A*, black bars). Preincubation of control fibers from NCD-fed mice with 1 μM Akt inhibitor VIII decreased the uptake of 2-NBDG stimulated by insulin, yielding 1.23 ± 0.15-fold stimulation compared with the 1.73 ± 0.04-fold stimulation produced by insulin alone (Fig. 4*A*, open bars). In fibers from HFD-fed mice, insulin scarcely stimulated the uptake of 2-NBDG, yielding values of 1.08 ± 0.04-fold stimulation, which were

Table 2. *Cholesterol content in skeletal muscle fibers isolated from control or HFD-fed mice*

Fibers	Without MβCD, μg cholesterol/mg protein	With MβCD, μg cholesterol/mg protein
NCD	5.45 ± 0.46	3.52 ± 0.52**
HFD	6.17 ± 0.51	3.55 ± 0.24**

Values are means ± SE. MβCD, methyl-β-cyclodextrin. Cholesterol levels were determined using Amplex Red fluorescence in fiber homogenates prepared from flexor digitorium brevis muscle. Incubation with 0.76 mM MβCD for 20 min reduced cholesterol levels in both NCD and HDF fibers. **$P < 0.01$, Student's *t*-test.

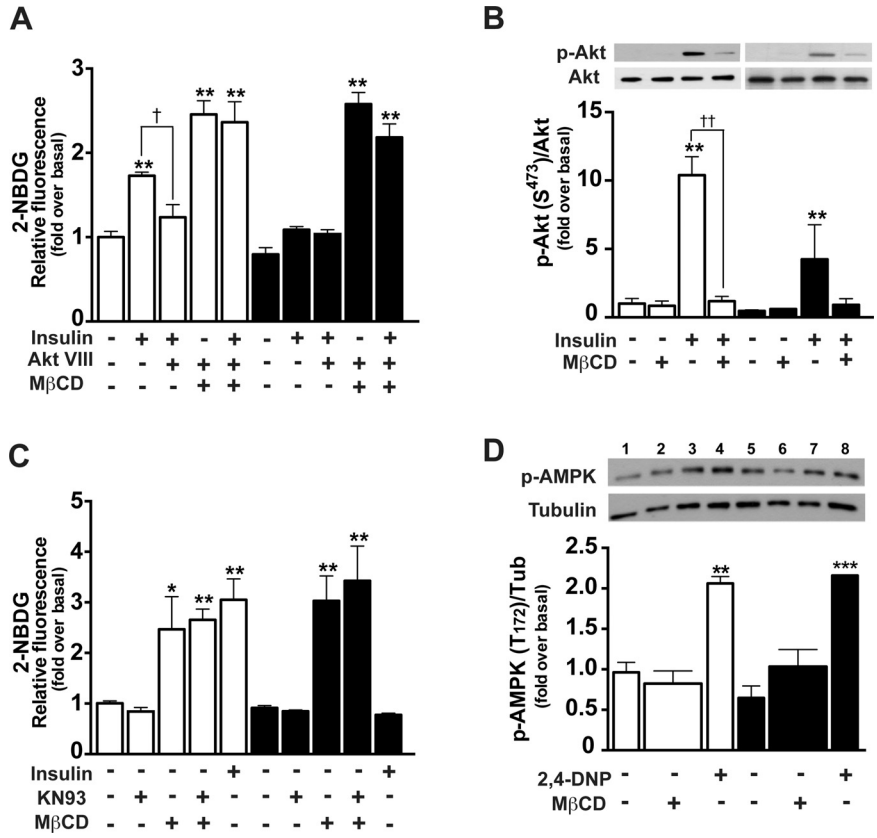

Fig. 4. Increased 2-NBDG uptake induced by MβCD persists after Akt or CaMK II/AMPK inhibition. Single fibers were preincubated with 300 μM 2-NBDG for 15 min before addition of insulin (100 nM) and/or MβCD (0.76 mM). *A*: effects of 1 μM Akt VIII on glucose transport (n = 3–5). Values are means ± SE. $^{**}P <$ 0.0001 vs. basal condition; $^{\dagger}P < 0.001$, determined by 1-way ANOVA plus Tukey's posttest. *B*: representative Western blot and quantification of p-Akt in Ser^{473} (n = 3–4). Values are means ± SE. $^{**}P < 0.0001$ vs. basal condition; $^{\dagger\dagger}P <$ 0.0001, determined by 1-way ANOVA plus Tukey's posttest. *C*: effects of 2 μM KN93 on glucose transport (n = 3–4). Values are means ± SE. $^{*}P < 0.001$; $^{**}P <$ 0.0001 vs. basal condition, determined by 1-way ANOVA plus Tukey's posttest. *D*: representative Western blot and quantification of p-AMPK in Thr^{172} (n = 3). For NCD mice, *lane 1*: basal condition; *lanes 2* and *3*: preincubated with 0.76 mM MβCD in basal condition (duplicate); *lane 4*: preincubated with 200 μM 2,4-dinitrophenol (2,4-DNP). For HFD-fed mice, *lane 5*: basal condition; *lanes 6* and *7*: preincubated with 0.76 mM MβCD in basal condition (duplicate); *lane 8*: preincubated with 200 μM 2,4-DNP. Quantifications of *lanes 2–3* and *6–7* are plotted as single bars. Values are means ± SE. $^{***}P <$ 0.0001; $^{**}P < 0.001$ vs. basal condition, determined by 1-way ANOVA plus Tukey's posttest.

similar to the values of 1.04 ± 0.06-fold stimulation determined in HFD fibers preincubated with 1 μM Akt inhibitor VIII plus insulin (Fig. 4*A*, black bars). To confirm these results, we measured the uptake of 2-NBDG in fibers preincubated with 1 μM MK-2206, an allosteric Akt inhibitor (23) that, in accord with the lack of effect of Akt inhibitor VIII, did not inhibit 2-NBDG uptake (data not shown). We measured next Akt phosphorylation in FDB whole muscle homogenates. As shown in Fig. 4*B* (open bars), preincubation of control fibers with 100 nM insulin promoted Akt phosphorylation in Ser^{473}, which was prevented by MβCD. In muscle homogenates from HFD-fed mice, insulin also promoted Akt phosphorylation in Ser^{473}, although the stimulation was lower than in controls; preincubation with MβCD eliminated the stimulation produced by insulin in control fibers (Fig. 4*B*, open bars). The inhibitory effects of MβCD on Akt phosphorylation might explain why the stimulatory effects of insulin on MβCD-induced 2-NBDG incorporation were not strictly the sum of the effects of MβCD and insulin by themselves.

We next tested the effects on 2-NBDG uptake of KN93, a potent, selective, and reversible inhibitor of AMPK-stimulated glucose uptake (27). Preincubation of control fibers with 1 μM KN93 did not modify MβCD-stimulated 2-NBDG uptake, yielding values of 2.46 ± 0.65-fold stimulation in fibers treated with MβCD and of 2.65 ± 0.21-fold in fibers preincubated with KN93 and MβCD (Fig. 4*C*, open bars). In HFD-fibers, we found values of 3.03 ± 0.49-fold stimulation by MβCD and of 3.42 ± 0.69-fold after preincubation with KN93 (Fig. 4*C*, black bars). In addition, we used Western blot assays to detect phosphorylated AMPK. After treatment with MβCD, we did not detect changes in the phosphorylation levels of Thr^{172} in muscle homogenates from NCD-fed mice, and there was a modest increase in muscle from HFD-fed mice; in contrast, 2,4-dinitrophenol (2,4-DNP) produced a significant increase in both muscle types (Fig. 4*D*). Altogether, our results suggest that MβCD activation of glucose uptake does not engage Akt or AMPK signaling pathways.

Indinavir inhibits MβCD-stimulated glucose uptake in CD and HFD muscle fibers. To assess whether GLUT4 transporters mediate the increased glucose uptake promoted by MβCD, we tested the effects of indinavir (100 μM), an antagonist of GLUT4 transporters used in the literature (50). Representative fluorescence images show that indinavir decreased the incorporation of 2-NBDG into muscle fibers from NCD- or HFD-fed mice treated with MβCD (Fig. 5*A*). Indinavir decreased to 1.14 ± 0.02-fold the stimulation produced by MβCD in fibers from NCD-fed mice, which in the absence of this inhibitor reached values of 2.21 ± 0.48 (Fig. 5*B*, open bars). In muscle fibers from HFD-fed mice, we found a similar effect; indinavir decreased from 2.22 ± 0.32 to 0.89 ± 0.09 the stimulation produced by MβCD (Fig. 5*B*, black bars). These results strongly suggest that MβCD increases the uptake of glucose via GLUT4 transporters.

MβCD increases GLUT4 translocation in muscle fiber membranes. To assess whether MβCD treatment promotes an increase in GLUT4 content in muscle membranes, we measured GLUT4 biotinylation as detailed in MATERIALS AND METHODS. As seen in the representative Western blot illustrated in Fig. 5*C*, treatment with 0.76 mM MβCD for 20 min produced a robust increase in GLUT4 biotinylation levels, an indication

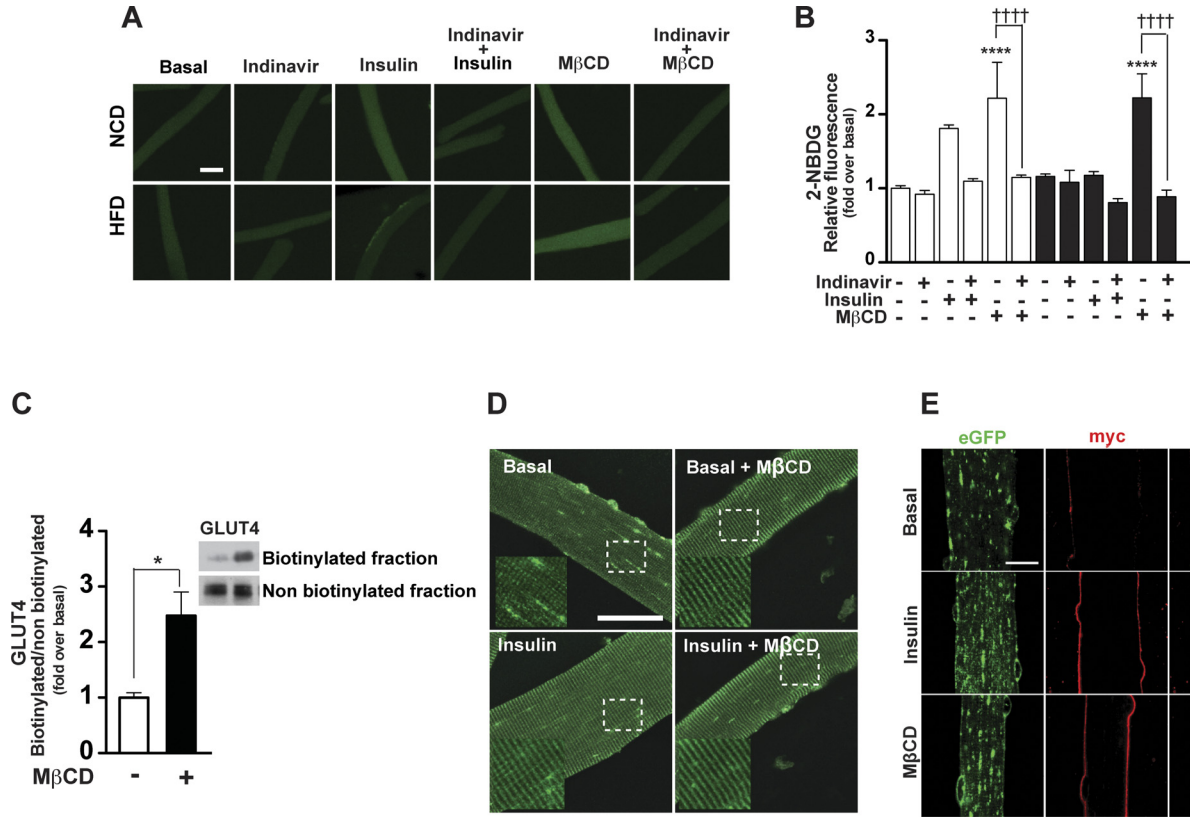

Fig. 5. Evidence supporting glucose transporter 4 (GLUT4) translocation induced by MβCD. *A*: representative images of indinavir's effects on probe fluorescence (n = 3–5). *B*: quantification of the effects of 100 μM indinavir. Open bars, NCD fibers; black bars, HFD fibers. Values are means ± SE. ****$P < 0.0001$ vs. basal condition; ††††$P < 0.0001$, determined by 1-way ANOVA plus Tukey's posttest. *C*: Western blot analysis of GLUT4 plasma membrane association evaluated by a biotinylation assay performed in NCD fibers (n = 3). *D*: confocal images of a representative experiment showing GLUT4 distribution analyzed by immunofluorescence in NCD fibers in the basal condition, preincubated with 0.76 mM MβCD, preincubated with 100 nM insulin, or preincubated with 0.76 mM MβCD + insulin (n = 3). *E*: confocal images of medial section (1 μm) were performed in NCD fibers from flexor digitorum brevis (FDB) muscle electroporated with the cDNA encode for the GLUT4*myc*-eGFP chimera. The *myc* epitope was detected with anti *myc* antibody (1:300) in nonpermeabilized fibers; anti-mouse Alexa fluor 546 nm was used as secondary antibody (1:600). The fibers were stimulated with the 546-nm laser beam, and the emission was collected with the 560-nm low-pass filter. The chimera-eGFP section was stimulated at 488 nm, and the emitted light was collected with the 500- to 530-nm band pass filter. (n = 3). Bars, 20 μm.

of surface exposure. In addition, preincubation with MβCD, insulin, or both promoted a change in GLUT4 localization in fibers from NCD-fed mice from a diffuse distribution to a striated pattern (Fig. 5*D*). To illustrate further the effect of MβCD in single fibers, we electroporated the FDB muscle with a plasmidial vector encoding the GLUT4*myc*-eGFP chimeric protein. This transporter has a *myc* epitope in its first extracellular loop and eGFP in the carboxy-terminal region. Isolated skeletal muscle fibers were stimulated with 100 nM insulin or 0.76 mM MβCD for 20 min, fixed, and incubated with anti-*myc* antibody in nonpermeabilized cells. In both experimental conditions a strong sarcolemmal fluorescence was detected, and the intracellular eGFP signal appeared to be redistributed in both cases (Fig. 5*E*).

Calcium dependence of MβCD-mediated glucose uptake. To examine in single fibers whether MβCD increases cytoplasmic calcium concentration, we loaded fibers with the fluorescence calcium indicator Fluo 4. We found that MβCD produced a calcium signal in both the presence (Fig. 6*A*, *graph i*) and the absence of extracellular calcium (Fig. 6*A*, *graph ii*), suggesting that MβCD produces a cytoplasmic calcium increase via calcium release from intracellular stores. The calcium signal appears to have two components: a fast component generated in the first few seconds, followed by a slower component that persisted for several min. Neither component changed in the presence or absence of extracellular calcium (Fig. 6*A*, bars at *right*). In skeletal muscle, the sarcoplasmic reticulum is the main intracellular calcium store. Xestospongin B, a known pharmacological inhibitor of the inositol 1,4,5-trisphosphate receptor, did not affect the calcium increase induced by MβCD (Fig. 6*A*, *graph iii*). In contrast, treatment with 100 μM dantrolene inhibited the MβCD-mediated calcium increase, suggesting that the calcium increase induced by MβCD requires RyR-mediated calcium release (Fig. 6*A*, *graph iv*).

To further investigate the role of RyR-mediated calcium release on MβCD-mediated glucose uptake, we measured glucose uptake in the presence of dantrolene. As illustrated in Fig. 6*B*, dantrolene inhibited basal glucose uptake, which decreased from the normalized value of 1.00 ± 0.03 to 0.77 ± 0.04; dantrolene also inhibited the stimulatory effect of MβCD on glucose uptake, which decreased from 1.67 ± 0.09 to 0.67 ± 0.04 (lower than in the basal condition). Taken together, our results suggest that MβCD stimulates RyR-mediated calcium release and that this calcium signal promotes GLUT4-mediated glucose uptake into the fibers.

DISCUSSION

In this study, we examined whether MβCD injection modifies plasma glucose levels and insulin sensitivity in HFD-fed mice, which represent a suitable experimental model of insulin resistance. We found that insulin sensitivity improved significantly after HFD-fed mice were injected with MβCD, a procedure that also restored plasma glucose concentration to normal levels. In addition, we investigated the effects of MβCD on GLUT4 translocation, glucose uptake, and calcium signal generation in adult skeletal muscle fibers. Our results indicate that acute incubation with MβCD, which roughly mimicked the effects of insulin, promoted RyR-mediated calcium release and increased glucose uptake in adult fibers isolated from both NCD- and HFD-fed mice.

Cholesterol plasma membrane content influences glucose transport. Earlier reports indicate that mammalian T-tubule membranes are highly enriched in cholesterol compared with the sarcolemma (49, 56). This feature likely contributes to the unusual physical properties of the T-tubule membrane system, which in its low fluidity at 37°C resembles more the membrane properties of a halophilic archaebacteria than those of other mammalian membranes (21). In response to insulin, the GLUT4 transporters translocate to the sarcolemma (46) and especially to the T-tubule system (38), a process that likely occurs in the cholesterol-enriched T-tubule lipid environment. We speculate that the findings presented here support a relationship between T-tubule membrane cholesterol content, where most GLUT4 translocation takes place, and GLUT4-mediated glucose transport. Our model predicts that lowering membrane cholesterol content would cause increased T-tubule membrane fluidity and possibly sarcolemmal membrane fluidity as well, resulting in enhanced insulin-mediated glucose transport, whereas increasing cholesterol levels would have the opposite effect. Previous reports support this hypothesis. After MβCD treatment, GLUT4*myc*-eGFP translocated to the sarcolemma, as shown by an important increase in fluorescence in the fiber surface; lack of T-tubule label is likely due to limited diffusion of the *myc* antibody within the fiber. However, the transfected carboxy-terminal eGFP segment shows rearrangement in its distribution, and some weak transverse fluorescence could be detected compared with the basal condition. Lowering cholesterol levels in leukemia cells promotes GLUT1 translocation toward the plasma membrane, suggesting that plasma membrane cholesterol depletion leads to glucose transport stimulation (7). Glucose-intolerant animal models and humans accumulate cholesterol in their skeletal muscle membranes (19). This observation correlates well with the results shown here, where we found increased cholesterol content in triads isolated from HFD-fed mice, which are insulin resistant. The high plasma membrane cholesterol content of 3T3-L1 adipocytes (37) and L6 myotubes cultured in the presence of fatty acids (19) decreases insulin-promoted glucose transport in these cells. Additionally, a recent report indicates that a high-fat diet reduces insulin signaling, abolishing phosphatidylinositol 3,4,5-phosphate production and GLUT4 translocation to

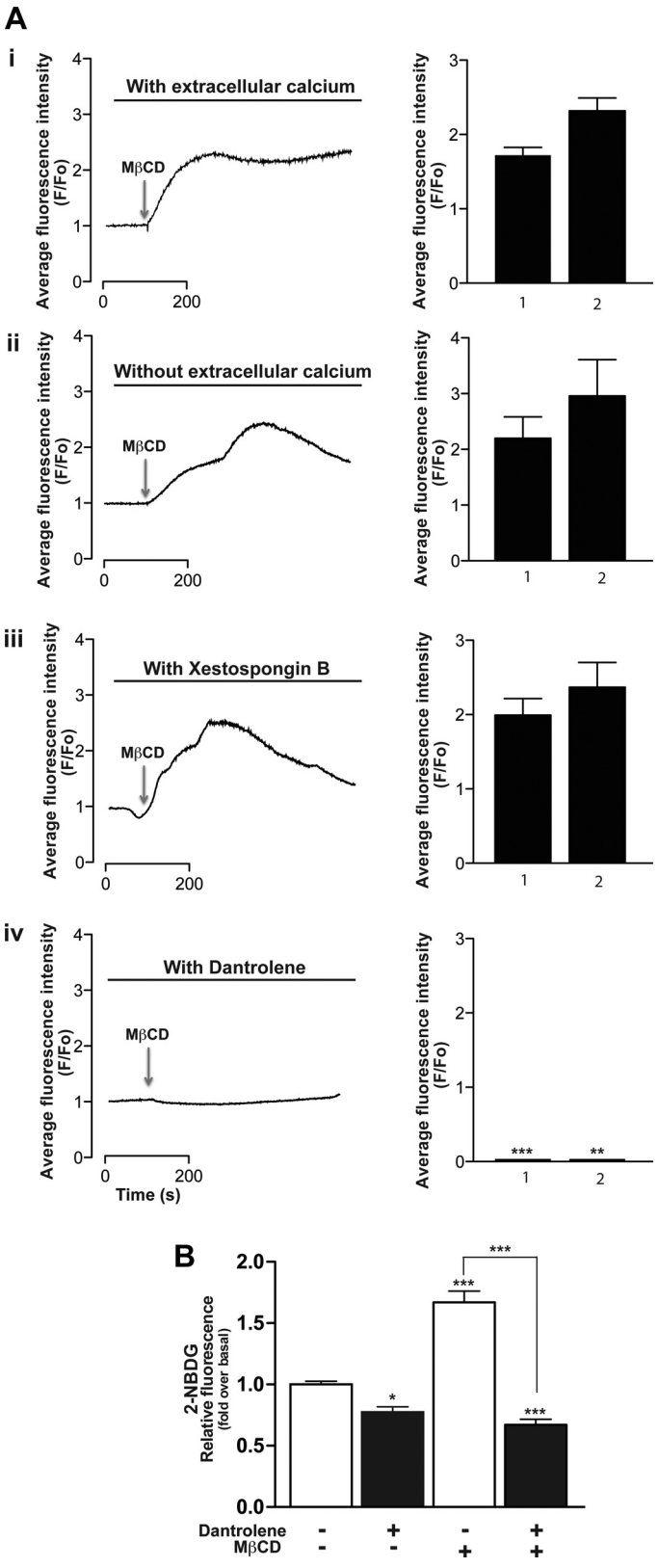

Fig. 6. MβCD generates calcium signals in isolated adult fibers. *A*: records of $[Ca^{2+}]_i$ vs. time obtained from single adult fibers preincubated for 30 min with Fluo 4-AM. Representative records were obtained in the presence (*graph i*) or absence (*graph ii*) of extracellular calcium or in fibers treated with 5 μM xestospongin B (*graph iii*) or 100 μM dantrolene (*graph iv*) (n = 5–7). The graphs on the *right* show the average fluorescence values of the first component as 1 and the second component as 2. *B*: 2-NBDG uptake (n = 3). Values represent means ± SE. $*P < 0.01$, $**P < 0.001$, and $***P < 0.0001$, determined by 1-way ANOVA plus Tukey's posttest.

the T-tubules of live mouse skeletal muscle (35). Moreover, treatment of 3T3-L1 adipocytes with chromium picolinate, a compound that removes membrane cholesterol, activates GLUT4 trafficking and enhances insulin-stimulated glucose transport via a cholesterol-dependent mechanism (10). In addition, treatment of adipocytes with increasing concentrations of MβCD reversibly decreases in dose-dependent fashion the cholesterol content of adipocyte membranes, leading to increased GLUT4 incorporation into the plasma membrane (37). Increased cholesterol levels in the plasma membrane may impair insulin action through modified F-actin structure and an increase in the hexosamine biosynthesis pathway (3). A previous report showed that the actin cytoskeleton, recognized to be essential in the regulation of GLUT4 translocation induced by insulin, is linked closely to cholesterol-enriched plasma membrane microdomains (24). However, we did not evaluate the possible involvement of F-actin and the hexosamine biosynthetic pathway on MβCD-mediated glucose uptake in adult skeletal muscle fibers.

A previous report showed that GLUT4 partially colocalizes with caveolin and that cholesterol depletion with MβCD, filipin, or cholesterol oxidase increases GLUT4 plasma membrane content in an insulin-independent manner (53). The GLUT4 transporter internalizes via either clathrin-mediated endocytocis or cholesterol-dependent but clathrin-independent endocytosis (16). In both adipocytes and L6 myotubes, the major route of endocytosis of GLUT4 is through clathrin-mediated endocytocis (16). A role for cholesterol-rich caveolae has been implicated in GLUT4 internalization in 3T3-L1 adipocytes (47). Importantly, MβCD inhibits caveolin-mediated endocytosis of GLUT4 in adipocytes (53). In highly differentiated and structured cells, such as adult muscle fibers, caveolin-mediated endocytosis may play a major role in GLUT4 endocytosis. We found that treatment of muscle fibers with MβCD increases GLUT4 content in the membrane and produces a change in GLUT4 localization. Indinavir interacts noncompetitively with GLUT4 and specifically inhibits GLUT4 function (40, 41, 50) and has been a useful tool to assess different functional contributions of GLUT4 to glucose uptake in skeletal muscle models and adipocytes (50). Our results show that indinavir inhibited MβCD-mediated glucose uptake, suggesting that the GLUT4 transporter mediates the enhanced glucose uptake induced by MβCD. However, we did not evaluate whether MβCD inhibits GLUT4 endocytosis or increases its exocytosis in adult fibers; future studies will allow us to evaluate and elucidate whether MβCD affects GLUT4 endocytosis, exocytosis, or both.

A recent report showed that AMPK mediates both cholesterol-dependent and cholesterol-independent regulation of GLUT4 translocation in L6 myotubes (18). Our results indicate that the CaMK II/AMPK inhibitor KN93 did not affect MβCD-mediated glucose uptake in either NCD- or HFD-fed mice. The PI3K pathway and Akt activation play well-established roles in GLUT4 vesicle trafficking to the cell membrane in response to insulin (62). However, our results indicate that the Akt inhibitors Akt VIII and MK-2206 did not affect MβCD-stimulated glucose uptake in adult skeletal muscle fibers from either NCD- or HFD-fed mice, suggesting that this pathway does not contribute to MβCD-induced stimulation. A different result has been reported in 3T3-L1 adipocytes and L6 muscle cell lines incubated with ceramides, suggesting that caveolin-enriched microdomains recruit and retain Akt in a cholesterol-dependent manner (20); activation of Akt by MβCD should be expected in that case. The present findings, showing lack of effect of Akt inhibitors on MβCD-stimulated glucose uptake, indicate that a different mechanism operates in adult skeletal muscle fibers where the T-tubule system is fully developed. Emerging evidence suggests participation of a novel, PI3K-independent pathway in glucose uptake. In adipocytes (26) and myotubes in culture (15), this pathway involves a G protein TC10-dependent signaling pathway but does not entail Akt activation. This cascade also involves the insulin receptor and the Cbl/C3G/TC10 pathway (9) and appears to occur within the specialized environment of lipid raft microdomains in the plasma membrane (15, 61). However, this novel pathway has been controversial, and the role of the Cbl/C3G/TC10 pathway in the modulation of GLUT4 translocation in adult skeletal muscle cells awaits elucidation.

Insulin-induced cytoplasmic calcium signals. We show here, through measurement of intracellular calcium in fibers, that MβCD induces an increase in cytoplasmic calcium levels. These results are physiologically relevant since an intracellular calcium increase is a likely requisite for contraction-mediated glucose uptake in skeletal muscle (48). The calcium ionophore A23187 increases glucose uptake in L6 myotubes (42) and primary myoblast cultures (52). In skeletal muscle fibers, Ca^{2+} influx is important for full stimulation of insulin-mediated glucose uptake (12, 30, 32). Nonetheless, the role played by cytoplasmic calcium signals on glucose uptake remains controversial. Earlier work suggested that calcium stimulates glucose transport in skeletal muscle by a pathway independent of contraction (64). In rat epitrochlearis muscle, raising intracellular Ca^{2+} by in vitro treatment with the RyR agonist caffeine increases glucose transport (57, 64). Dantrolene, an inhibitor of the interaction between Cav1.1 and RyR1(1), inhibits GLUT4 trafficking to the plasma membrane via a Ca^{2+}-dependent mechanism and prevents insulin-dependent glucose uptake in adipocytes (36). We found that dantrolene inhibits MβCD-mediated glucose uptake, suggesting that MβCD stimulates insulin-independent intracellular Ca^{2+} signaling in skeletal muscle fibers via stimulation of RyR-mediated Ca^{2+} release. We propose that the cytoplasmic calcium rise induced by MβCD increases GLUT4 translocation to the cell surface, leading to the consequent stimulation of glucose uptake.

Previous studies indicate that calcium signals may be relevant for the late steps in the insulin-signaling pathway, enabling docking and fusion of GLUT4-containing vesicles to the membrane (31). Recently, it has been reported in live adipocytes that the 138-kDa C2 domain-containing phosphoprotein (CDP138) is required for optimal insulin-stimulated glucose transport, GLUT4 translocation, and fusion of GLUT4-containing vesicles with the plasma membrane (63). The purified C2 domain of CDP138 binds Ca^{2+} and lipid membranes (63). In addition, studies in vitro have shown that the cytoplasmic protein Doc2b, which possesses two homologous C2 domains, promotes GLUT4 exocytosis by activating the SNARE-mediated fusion reaction in a calcium- and membrane-bending-dependent manner (65). Yet the mechanisms by which intracellular calcium signals promote GLUT4 translocation to the T-tubule and surface membranes and the subsequent increase in glucose transport remain largely unknown.

Cholesterol lowering with MβCD decreases insulin resistance. The use of controlled manipulation of membrane cholesterol content has increased sharply in the past years, especially as a method of studying putative cholesterol-enriched cell membrane domains (66). Various agents have been developed for the treatment of type 2 diabetes mellitus and insulin resistance; however, due to the increased population suffering from these diseases, it is important to find new therapeutic targets. The lowering of cholesterol accumulation in skeletal muscle membranes could be one of them. We used MβCD, a cyclic oligosaccharide consisting of seven β-(1–4)-glucopyranose rings, to remove cholesterol from adult skeletal fibers in vitro using HFD-fed mice as an experimental model of insulin resistance. The exact mechanism by which MβCD removes cholesterol from cells remains incompletely understood, but the formation of cholesterol/MβCD inclusion complexes at the membrane surface is a widely accepted option (66). Here, we showed that MβCD has beneficial effects on plasma glucose levels in HFD-fed mice. MβCD has biomedical and pharmaceutical interests and has been used in vivo with nontoxic effects (55); it has recently received FDA approval for the treatment of Niemann-Pick and Tangier diseases (60) and has been suggested as a potential novel treatment of diabetic nephropathy (39). Accordingly, MβCD and its derivatives should be tested as possible drugs to treat insulin resistance.

In conclusion, our findings imply a novel role for both T-tubule cholesterol content and intracellular calcium transients on GLUT4 translocation and glucose transport in adult skeletal muscle and suggest that partial cholesterol removal from muscle fibers with MβCD may be a possible novel therapeutic strategy to treat insulin resistance. To understand how cholesterol accumulates in skeletal muscle and how MβCD-mediated cholesterol removal alters specific cell functions will require further mechanistic studies.

ACKNOWLEDGMENTS

We thank Dr. José Luis Valdés for help with the mouse activity measurements.

This work was previously presented as abstract in *FASEB J* 26: 759.12, 2012, and *FASEB J* 27: 1109.3, 2013.

GRANTS

This work was financed by Fondo Nacional de Desarrollo Científico y Tecnológico Grants 3110105 (P. Llanos), 11130267 (A. Contreras-Ferrat), and ACT-1111 (E. Jaimovich) and the Scholarship from the German Academic Exchange Service (T. Georgiev). The funding agencies had no role in study design, data collection and analysis, decision to publish, or preparation of this article.

DISCLOSURES

The authors have declared that no competing interests, financial or otherwise, exist.

AUTHOR CONTRIBUTIONS

P.L. and E.J. conception and design of research; P.L., A.C.-F., T.G., C.O.-F., A.E., and J.H. performed experiments; P.L., A.C.-F., T.G., C.O.-F., and E.J. analyzed data; P.L., A.C.-F., A.E., and E.J. interpreted results of experiments; P.L. and T.G. prepared figures; P.L., C.H., and E.J. drafted manuscript; P.L., J.H., C.H., and E.J. edited and revised manuscript; P.L., J.H., C.H., and E.J. approved final version of manuscript.

REFERENCES

1. **Bannister RA, Pessah IN, Beam KG.** The skeletal L-type Ca(2+) current is a major contributor to excitation-coupled Ca(2+) entry. *J Gen Physiol* 133: 79–91, 2009.
2. **Berridge MJ, Bootman MD, Roderick HL.** Calcium signalling: dynamics, homeostasis and remodelling. *Nat Rev Mol Cell Biol* 4: 517–529, 2003.
3. **Bhonagiri P, Pattar GR, Habegger KM, McCarthy AM, Tackett L, Elmendorf JS.** Evidence coupling increased hexosamine biosynthesis pathway activity to membrane cholesterol toxicity and cortical filamentous actin derangement contributing to cellular insulin resistance. *Endocrinology* 152: 3373–3384, 2011.
4. **Bruton JD, Katz A, Westerblad H.** Insulin increases near-membrane but not global Ca2+ in isolated skeletal muscle. *Proc Natl Acad Sci USA* 96: 3281–3286, 1999.
5. **Bruton JD, Katz A, Westerblad H.** The role of Ca2+ and calmodulin in insulin signalling in mammalian skeletal muscle. *Acta Physiol Scand* 171: 259–265, 2001.
6. **Bryant NJ, Govers R, James DE.** Regulated transport of the glucose transporter GLUT4. *Nat Rev Mol Cell Biol* 3: 267–277, 2002.
7. **Caliceti C, Zambonin L, Prata C, Vieceli Dalla Sega F, Hakim G, Hrelia S, Fiorentini D.** Effect of plasma membrane cholesterol depletion on glucose transport regulation in leukemia cells. *PLoS One* 7: e41246, 2012.
8. **Casas M, Figueroa R, Jorquera G, Escobar M, Molgo J, Jaimovich E.** IP(3)-dependent, post-tetanic calcium transients induced by electrostimulation of adult skeletal muscle fibers. *J Gen Physiol* 136: 455–467, 2010.
9. **Chang L, Chiang SH, Saltiel AR.** Insulin signaling and the regulation of glucose transport. *Mol Med* 10: 65–71, 2004.
10. **Chen G, Liu P, Pattar GR, Tackett L, Bhonagiri P, Strawbridge AB, Elmendorf JS.** Chromium activates glucose transporter 4 trafficking and enhances insulin-stimulated glucose transport in 3T3-L1 adipocytes via a cholesterol-dependent mechanism. *Mol Endocrinol* 20: 857–870, 2006.
11. **Cheng D.** Prevalence, predisposition and prevention of type II diabetes. *Nutr Metab (Lond)* 2: 29, 2005.
12. **Contreras-Ferrat A, Llanos P, Vásquez C, Espinosa A, Osorio-Fuentealba C, Arias-Calderon M, Lavandero S, Klip A, Hidalgo C, Jaimovich E.** Insulin elicits a ROS-activated and an IP3-dependent Ca2+ release, which both impinge on GLUT4 translocation. *J Cell Sci* 127: 1911–1923, 2014.
13. **DiFranco M, Neco P, Capote J, Meera P, Vergara JL.** Quantitative evaluation of mammalian skeletal muscle as a heterologous protein expression system. *Protein Expr Purif* 47: 281–288, 2006.
14. **Espinosa A, Leiva A, Pena M, Muller M, Debandi A, Hidalgo C, Carrasco MA, Jaimovich E.** Myotube depolarization generates reactive oxygen species through NAD(P)H oxidase; ROS-elicited Ca2+ stimulates ERK, CREB, early genes. *J Cell Physiol* 209: 379–388, 2006.
15. **Fecchi K, Volonte D, Hezel MP, Schmeck K, Galbiati F.** Spatial and temporal regulation of GLUT4 translocation by flotillin-1 and caveolin-3 in skeletal muscle cells. *FASEB J* 20: 705–707, 2006.
16. **Foley K, Boguslavsky S, Klip A.** Endocytosis, recycling, and regulated exocytosis of glucose transporter 4. *Biochemistry* 50: 3048–3061, 2011.
17. **Green CJ, Goransson O, Kular GS, Leslie NR, Gray A, Alessi DR, Sakamoto K, Hundal HS.** Use of Akt inhibitor and a drug-resistant mutant validates a critical role for protein kinase B/Akt in the insulin-dependent regulation of glucose and system A amino acid uptake. *J Biol Chem* 283: 27653–27667, 2008.
18. **Habegger KM, Hoffman NJ, Ridenour CM, Brozinick JT, Elmendorf JS.** AMPK enhances insulin-stimulated GLUT4 regulation via lowering membrane cholesterol. *Endocrinology* 153: 2130–2141, 2012.
19. **Habegger KM, Penque BA, Sealls W, Tackett L, Bell LN, Blue EK, Gallagher PJ, Sturek M, Alloosh MA, Steinberg HO, Considine RV, Elmendorf JS.** Fat-induced membrane cholesterol accrual provokes cortical filamentous actin destabilisation and glucose transport dysfunction in skeletal muscle. *Diabetologia* 55: 457–467, 2012.
20. **Hajduch E, Turban S, Le Liepvre X, Le Lay S, Lipina C, Dimopoulos N, Dugail I, Hundal HS.** Targeting of PKCzeta and PKB to caveolin-enriched microdomains represents a crucial step underpinning the disruption in PKB-directed signalling by ceramide. *Biochem J* 410: 369–379, 2008.
21. **Hidalgo C.** Lipid phase of transverse tubule membranes from skeletal muscle. An electron paramagnetic resonance study. *Biophys J* 47: 757–764, 1985.

22. **Hidalgo C, Jorquera J, Tapia V, Donoso P.** Triads and transverse tubules isolated from skeletal muscle contain high levels of inositol 1,4,5-trisphosphate. *J Biol Chem* 268: 15111–15117, 1993.
23. **Hirai H, Sootome H, Nakatsuru Y, Miyama K, Taguchi S, Tsujioka K, Ueno Y, Hatch H, Majumder PK, Pan BS, Kotani H.** MK-2206, an allosteric Akt inhibitor, enhances antitumor efficacy by standard chemotherapeutic agents or molecular targeted drugs in vitro and in vivo. *Mol Cancer Ther* 9: 1956–1967, 2010.
24. **Hoffman NJ, Elmendorf JS.** Signaling, cytoskeletal and membrane mechanisms regulating GLUT4 exocytosis. *Trends Endocrinol Metab* 22: 110–116, 2011.
25. **Huang S, Czech MP.** The GLUT4 glucose transporter. *Cell Metab* 5: 237–252, 2007.
26. **JeBailey L, Rudich A, Huang X, Di Ciano-Oliveira C, Kapus A, Klip A.** Skeletal muscle cells and adipocytes differ in their reliance on TC10 and Rac for insulin-induced actin remodeling. *Mol Endocrinol* 18: 359–372, 2004.
27. **Jensen TE, Rose AJ, Hellsten Y, Wojtaszewski JF, Richter EA.** Caffeine-induced Ca^{2+} release increases AMPK-dependent glucose uptake in rodent soleus muscle. *Am J Physiol Endocrinol Metab* 293: E286–E292, 2007.
28. **Kelley DE, Mandarino LJ.** Fuel selection in human skeletal muscle in insulin resistance: a reexamination. *Diabetes* 49: 677–683, 2000.
29. **Kewalramani G, Bilan PJ, Klip A.** Muscle insulin resistance: assault by lipids, cytokines and local macrophages. *Curr Opin Clin Nutr Metab Care* 13: 382–390, 2010.
30. **Lanner JT, Bruton JD, Assefaw-Redda Y, Andronache Z, Zhang SJ, Severa D, Zhang ZB, Melzer W, Zhang SL, Katz A, Westerblad H.** Knockdown of TRPC3 with siRNA coupled to carbon nanotubes results in decreased insulin-mediated glucose uptake in adult skeletal muscle cells. *FASEB J* 23: 1728–1738, 2009.
31. **Lanner JT, Bruton JD, Katz A, Westerblad H.** Ca(2+) and insulin-mediated glucose uptake. *Curr Opin Pharmacol* 8: 339–345, 2008.
32. **Lanner JT, Katz A, Tavi P, Sandstrom ME, Zhang SJ, Wretman C, James S, Fauconnier J, Lannergren J, Bruton JD, Westerblad H.** The role of Ca2+ influx for insulin-mediated glucose uptake in skeletal muscle. *Diabetes* 55: 2077–2083, 2006.
33. **Larance M, Ramm G, James DE.** The GLUT4 code. *Mol Endocrinol* 22: 226–233, 2008.
34. **Lau YH, Caswell AH, Brunschwig JP, Baerwald R, Garcia M.** Lipid analysis and freeze-fracture studies on isolated transverse tubules and sarcoplasmic reticulum subfractions of skeletal muscle. *J Biol Chem* 254: 540–546, 1979.
35. **Lauritzen HP, Ploug T, Ai H, Donsmark M, Prats C, Galbo H.** Denervation and high-fat diet reduce insulin signaling in T-tubules in skeletal muscle of living mice. *Diabetes* 57: 13–23, 2008.
36. **Li Y, Wang P, Xu J, Desir GV.** Voltage-gated potassium channel Kv1.3 regulates GLUT4 trafficking to the plasma membrane via a Ca^{2+}-dependent mechanism. *Am J Physiol Cell Physiol* 290: C345–C351, 2006.
37. **Liu P, Leffler BJ, Weeks LK, Chen G, Bouchard CM, Strawbridge AB, Elmendorf JS.** Sphingomyelinase activates GLUT4 translocation via a cholesterol-dependent mechanism. *Am J Physiol Cell Physiol* 286: C317–C329, 2004.
38. **Marette A, Burdett E, Douen A, Vranic M, Klip A.** Insulin induces the translocation of GLUT4 from a unique intracellular organelle to transverse tubules in rat skeletal muscle. *Diabetes* 41: 1562–1569, 1992.
39. **Merscher-Gomez S, Guzman J, Pedigo CE, Lehto M, Aguillon-Prada R, Mendez A, Lassenius MI, Forsblom C, Yoo T, Villarreal R, Maiguel D, Johnson K, Goldberg R, Nair V, Randolph A, Kretzler M, Nelson RG, Burke GW 3rd, Groop PH, Fornoni A; FinnDiane Study Group.** Cyclodextrin protects podocytes in diabetic kidney disease. *Diabetes* 62: 3817–3827, 2013.
40. **Murata H, Hruz PW, Mueckler M.** Indinavir inhibits the glucose transporter isoform Glut4 at physiologic concentrations. *AIDS* 16: 859–863, 2002.
41. **Murata H, Hruz PW, Mueckler M.** The mechanism of insulin resistance caused by HIV protease inhibitor therapy. *J Biol Chem* 275: 20251–20254, 2000.
42. **Oberg AI, Yassin K, Csikasz RI, Dehvari N, Shabalina IG, Hutchinson DS, Wilcke M, Ostenson CG, Bengtsson T.** Shikonin increases glucose uptake in skeletal muscle cells and improves plasma glucose levels in diabetic Goto-Kakizaki rats. *PLoS One* 6: e22510, 2011.
43. **Ohtani Y, Irie T, Uekama K, Fukunaga K, Pitha J.** Differential effects of alpha-, beta- and gamma-cyclodextrins on human erythrocytes. *Eur J Biochem* 186: 17–22, 1989.
44. **Osorio-Fuentealba C, Contreras-Ferrat AE, Altamirano F, Espinosa A, Li Q, Niu W, Lavandero S, Klip A, Jaimovich E.** Electrical stimuli release ATP to increase GLUT4 translocation and glucose uptake via PI3Kgamma-Akt-AS160 in skeletal muscle cells. *Diabetes* 62: 1519–1526, 2013.
45. **Pessin JE, Saltiel AR.** Signaling pathways in insulin action: molecular targets of insulin resistance. *J Clin Invest* 106: 165–169, 2000.
46. **Ploug T, van Deurs B, Ai H, Cushman SW, Ralston E.** Analysis of GLUT4 distribution in whole skeletal muscle fibers: identification of distinct storage compartments that are recruited by insulin and muscle contractions. *J Cell Biol* 142: 1429–1446, 1998.
47. **Ros-Baro A, Lopez-Iglesias C, Peiro S, Bellido D, Palacin M, Zorzano A, Camps M.** Lipid rafts are required for GLUT4 internalization in adipose cells. *Proc Natl Acad Sci USA* 98: 12050–12055, 2001.
48. **Rose AJ, Richter EA.** Skeletal muscle glucose uptake during exercise: how is it regulated? *Physiology (Bethesda)* 20: 260–270, 2005.
49. **Rosemblatt M, Hidalgo C, Vergara C, Ikemoto N.** Immunological and biochemical properties of transverse tubule membranes isolated from rabbit skeletal muscle. *J Biol Chem* 256: 8140–8148, 1981.
50. **Rudich A, Konrad D, Torok D, Ben-Romano R, Huang C, Niu W, Garg RR, Wijesekara N, Germinario RJ, Bilan PJ, Klip A.** Indinavir uncovers different contributions of GLUT4 and GLUT1 towards glucose uptake in muscle and fat cells and tissues. *Diabetologia* 46: 649–658, 2003.
51. **Saltiel AR.** New perspectives into the molecular pathogenesis and treatment of type 2 diabetes. *Cell* 104: 517–529, 2001.
52. **Schudt C, Gaertner U, Pette D.** Insulin action on glucose transport and calcium fluxes in developing muscle cells in vitro. *Eur J Biochem* 68: 103–111, 1976.
53. **Shigematsu S, Watson RT, Khan AH, Pessin JE.** The adipocyte plasma membrane caveolin functional/structural organization is necessary for the efficient endocytosis of GLUT4. *J Biol Chem* 278: 10683–10690, 2003.
54. **Shulman GI.** Cellular mechanisms of insulin resistance. *J Clin Invest* 106: 171–176, 2000.
55. **Stella VJ, He Q.** Cyclodextrins. *Toxicol Pathol* 36: 30–42, 2008.
56. **Sumnicht GE, Sabbadini RA.** Lipid composition of transverse tubular membranes from normal and dystrophic skeletal muscle. *Arch Biochem Biophys* 215: 628–637, 1982.
57. **Terada S, Muraoka I, Tabata I.** Changes in $[Ca^{2+}]_i$ induced by several glucose transport-enhancing stimuli in rat epitrochlearis muscle. *J Appl Physiol (1985)* 94: 1813–1820, 2003.
58. **Thiebaud D, Jacot E, DeFronzo RA, Maeder E, Jequier E, Felber JP.** The effect of graded doses of insulin on total glucose uptake, glucose oxidation, and glucose storage in man. *Diabetes* 31: 957–963, 1982.
59. **Thong FS, Dugani CB, Klip A.** Turning signals on and off: GLUT4 traffic in the insulin-signaling highway. *Physiology (Bethesda)* 20: 271–284, 2005.
60. **Tufro A.** Cholesterol accumulation in podocytes: a potential novel targetable pathway in diabetic nephropathy. *Diabetes* 62: 3661–3662, 2013.
61. **Watson RT, Pessin JE.** Subcellular compartmentalization and trafficking of the insulin-responsive glucose transporter, GLUT4. *Exp Cell Res* 271: 75–83, 2001.
62. **Welsh GI, Hers I, Berwick DC, Dell G, Wherlock M, Birkin R, Leney S, Tavare JM.** Role of protein kinase B in insulin-regulated glucose uptake. *Biochem Soc Trans* 33: 346–349, 2005.
63. **Xie X, Gong Z, Mansuy-Aubert V, Zhou QL, Tatulian SA, Sehrt D, Gnad F, Brill LM, Motamedchaboki K, Chen Y, Czech MP, Mann M, Kruger M, Jiang ZY.** C2 domain-containing phosphoprotein CDP138 regulates GLUT4 insertion into the plasma membrane. *Cell Metab* 14: 378–389, 2011.
64. **Youn JH, Gulve EA, Holloszy JO.** Calcium stimulates glucose transport in skeletal muscle by a pathway independent of contraction. *Am J Physiol Cell Physiol* 260: C555–C561, 1991.
65. **Yu H, Rathore SS, Davis EM, Ouyang Y, Shen J.** Doc2b promotes GLUT4 exocytosis by activating the SNARE-mediated fusion reaction in a calcium- and membrane bending-dependent manner. *Mol Biol Cell* 24: 1176–1184, 2013.
66. **Zidovetzki R, Levitan I.** Use of cyclodextrins to manipulate plasma membrane cholesterol content: evidence, misconceptions and control strategies. *Biochim Biophys Acta* 1768: 1311–1324, 2007.